Applied Energy 281 (2021) 116048

Contents lists available at ScienceDirect

Applied Energy

journal homepage: www.elsevier.com/locate/apenergy

Atmospheric pressure gradients and Coriolis forces provide geophysical limits to power density of large wind farms

Enrico G.A. Antonini *, Ken Caldeira

Carnegie Institution for Science, Department of Global Ecology, Stanford, CA, USA

HIGHLIGHTS

- We provide a theoretical basis for upper limits of power density in large wind farms.
- Pressure gradients within the Ekman layer supply energy to large wind power plants.
- Interacting pressure-gradient, Coriolis and drag forces control the power density.
- The power density of regional-scale wind farms is resource- and geographic-dependent.

ARTICLE INFO

Keywords:
Wind farm efficiency
Power density
Geophysical limits
Coriolis force
Pressure gradient
Turbine-atmosphere interaction

ABSTRACT

The geophysical limit to maximum land-area power density of large wind farms is related to the rate of replenishment of kinetic energy removed from the atmosphere by wind turbines. Although observations and numerical simulations have indicated an upper bound to the power density in the order of 1 W/m^2, no theoretical foundation has yet been provided. Here, we study the role of atmospheric pressure gradients and the latitude-dependent Coriolis parameter in the power density of large-scale wind farms by means of both numerical atmospheric simulations and analytic expressions. We illustrate that energy transport to regional-scale wind farms is primarily governed by horizontal pressure gradients and their interaction with the Coriolis force and turbine-induced surface drag within the latitude-dependent Ekman layer. Higher pressure gradients and lower Coriolis parameters promote higher energy availability and, consequently, higher potential power density, suggesting that the power density of regional-scale wind farms is largely resource- and location-dependent.

1. Introduction

Wind energy has been one of the fastest growing renewable energy technologies [1], driven in part by demand for low or net-zero emission energy systems to address climate change [2,3], increasing government support [4,5] and public receptiveness [6,7]. The worldwide share of electricity generated from wind in 2018 amounted to just 4.6% [1], but its growth has been exponential over the past decades, and some current projections see wind energy's share reaching one-quarter to one-third globally by 2050 [8]. In such scenarios, wind farms are expected to increase both in number and spatial scale.

Understanding the physics regulating the performance of large-scale wind farms is one of the current challenges in wind energy science [9,10]. A parameter used to characterize the performance of wind farms is power density, defined as the ratio between the average power generation and the wind farm's land area. Studies of large-scale wind farms have suggested that maximum power density is limited by the downward transport of kinetic energy from the upper troposphere [11–13]. Numerical and observation-based studies have estimated maximum wind farm power densities to be about 1 W/m^2 for on-shore [14–16] and between 3 and 6 W/m^2 for some off-shore locations [17,18]. The qualitative dependence of wind farm power density on several atmospheric characteristics and phenomena is well understood: first and most cleary, higher winds promote higher energy generations; atmospheric turbulence increases energy transport [19–22]; heat fluxes may increase or suppress turbulence, depending on their direction [23–26]. Geometric properties such as terrain topography and surface roughness [17,27–29], turbine characteristics and spatial arrangement [30–33] also play a role in the wind farm energy generation. However, theoretical frameworks that give a clear relation of these quantities with

* Corresponding author.
E-mail address: eantonini@carnegiescience.edu (E.G.A. Antonini).

https://doi.org/10.1016/j.apenergy.2020.116048
Received 18 June 2020; Received in revised form 11 October 2020; Accepted 17 October 2020
Available online 1 November 2020

wind farm performance are lacking, especially for spatial scales for which the latitude-dependent Coriolis force, pressure-gradient force, and other larger-scale atmospheric physics are important. Miller *et al.* [14] developed a method to estimate the wind farm maximum energy extraction from the vertical downward flux of kinetic energy from the atmosphere considering pre-turbine climatology in central Kansas, USA. Luzzatto-Fegiz *et al.* [34] developed a simplified expression for the power density of large-scale wind farms (considered as an idealized infinite array) as a function of the overlying wind speed, atmospheric turbulence and stability. Both these studies provided useful insight into the energy transport in wind farms, but neglected the importance of the pressure-gradient and Coriolis forces and their role in transporting energy to large-scale wind farms. Further, there has been little theoretical understanding of the sources of energy and momentum that replenish the energy and momentum extracted by wind turbines.

Here, we study the role of horizontal pressure gradients and the Coriolis parameter in the power density of large-scale wind farms by means of both numerical atmospheric simulations and analytic expressions. The latter combine governing equations from atmospheric fluid dynamics (particularly, the Ekman layer equations) and wind farm fluid dynamics to give a closed-form relation that ultimately can be used to estimate the power density of large-scale wind farms. Our analysis shows that the replenishment of energy and momentum extracted by large-scale wind farms is governed by horizontal pressure-gradient and Coriolis forces. The energy is supplied by the pressure-gradient force within the Ekman layer and transported downward to the turbines; it does not originate from the overlying free troposphere (above the planetary boundary layer) as previously suggested. We show that regions with higher horizontal pressure gradients have higher energy availability and, consequently, higher energy generation per unit surface area. We also show that, for the same horizontal pressure gradient, the power density is higher in lower latitudes, suggesting that the replenishment rate of kinetic energy depends also on the degree to which the pressure-gradient force is opposed by the Coriolis force. Given the lack of theoretical understanding of large-scale wind farm performance, this study provides both theoretical understanding and a numerical approximation of the upper limits to energy extraction for large wind farms that is relevant to the planning and economic evaluation of such systems.

2. The role of pressure gradients and the Coriolis parameter

To study the role of pressure gradients and the latitude-dependent Coriolis parameter in the power density of large-scale wind farms, we consider a representative, idealized scenario in which a wind farm extends infinitely (Fig. 1). This configuration has been used to study such large systems [11,34] because it enables to focus only on the vertical transport of momentum and kinetic energy, underlying a statistical horizontal homogeneity and negligible horizontal fluxes. It is implicit that such representation would not be valid for small-scale systems where horizontal fluxes of momentum and kinetic energy become comparable to the vertical ones.

If we imagine an infinite wind farm on the surface of a plane with winds aloft, in a non-rotating environment and driven only by a pressure-gradient force, $-1/\rho\nabla p$, the wind would flow down the pressure gradient. Winds close to the surface would be slowed by the drag of the wind turbines and follow a log-like profile with altitude. Energy would get to the wind turbines supplied by the pressure-gradient force and through downward transport of energy through the vertical column [35]. Now imagine that we add to this picture a Coriolis force that originates from the Earth's rotation, fG, where f is the Coriolis parameter and G the geostrophic wind. The winds aloft, far enough from the wind turbine array, would not feel the surface drag and then create a geostrophic balance: the pressure gradient would be orthogonal to the direction of wind flow and in balance with the apparent Coriolis force. In this setting, forces would be perpendicular to the air motion and no energy would be exchanged. When winds close to the surface are slowed because of the drag, the apparent Coriolis force would be reduced and no longer balance the pressure-gradient force [36]. The wind flow would no longer be orthogonal to the pressure-gradient force, and this force would then be able to impart energy to the system. Thus, when the apparent Coriolis force acts on the system, there is a local energy source given by the large-scale available potential energy provided by the pressure field. We postulate that the local deviation of air flow from the main geostrophic direction controls the energy that reaches the wind turbines and, accordingly, that the power density is largely controlled by horizontal pressure gradients, which drive geostrophic winds, and latitude.

We characterize the power density of an idealized large wind farm (Fig. 1) under the following assumptions: in the upper part of the

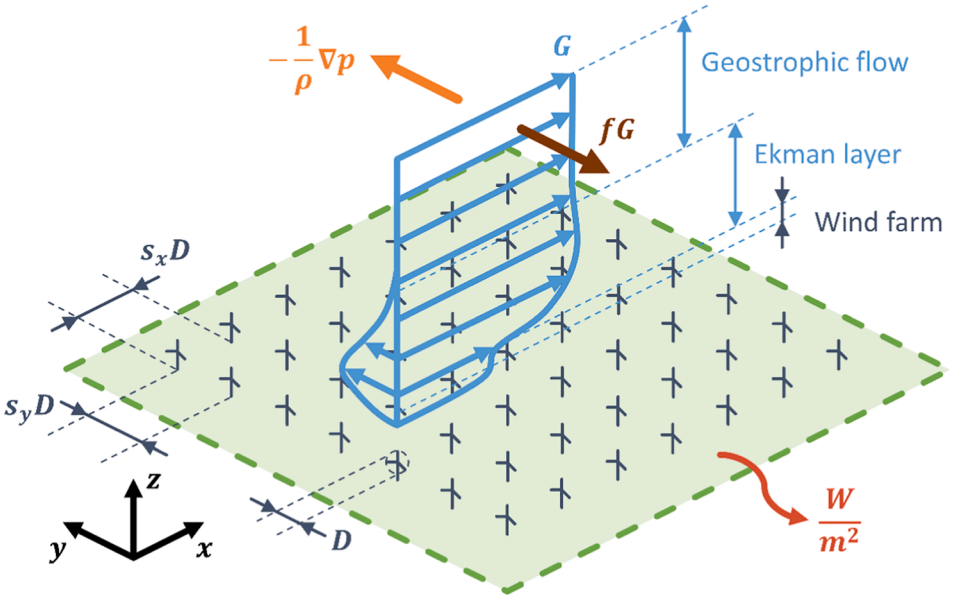

Fig. 1. An illustration of the fundamental phenomena and parameters that govern the energy extraction of large-scale wind farms. The geostrophic wind, G, is the result of the balance between the pressure-gradient force, $-1/\rho\nabla p$, and the Coriolis force, fG, where f is the Coriolis parameter. Wind turbines of diameter D are arranged on a regular grid with horizontal spacings of dimensions s_xD and s_yD. The power density of the wind farm is expressed in W/m^2.

troposphere, a geostrophic flow results from the balance of the pressure-gradient force and the Coriolis force; between the overlying geostrophic flow and the underlying wind farm, an Ekman layer results from the balance of the pressure-gradient force, Coriolis force and turbulent-flux divergence [36]. In statistically steady and homogeneous flows, momentum and kinetic energy are transported downward through the Ekman layer, and the energy extracted by the turbines is continuously replenished [11,37]. If wind turbine geometry, performance (provided by the manufacturer), and arrangement are known, and neutral atmospheric conditions (i.e., no thermal convection or stratification) and dry air are assumed, the two parameters that drive this system and the energy exchange are the pressure-gradient force and the latitude-dependent Coriolis parameter.

We study this system using two different approaches. The first one employs atmospheric simulations conducted with the Weather Research and Forecasting (WRF) simulation tool [38], where the wind turbines are parametrized as sinks of momentum and sources of turbulence kinetic energy [39–41]. Here, we consider a wind farm with a set of Vestas V164-9.0 MW (see Supplementary Note 1), one of the largest wind turbines currently available, arranged on a uniform grid with spacing of 1000 m. We populate this uniform grid with turbines to obtain and study two different installed capacity densities: 9 W/m^2, where all the grid cells contain a turbine resulting in an aligned layout with a turbine density of 1 km^{-2}, and 4.5 W/m^2, where the grid cells are populated alternatively resulting in a staggered layout with a turbine density of 0.5 km^{-2}. We parametrize this wind farm on the bottom layers of a doubly periodic, limited computational domain that we use to emulate an infinite wind farm. On this domain, we specify a set of vertically uniform geostrophic wind values and constant Coriolis parameters (f-plane approximation) to understand how varying these two parameters would affect the performance of large-scale wind farms. These settings in the boundary conditions implicitly assume a driving constant pressure-gradient field for each of the considered combinations (see Methods in Sec. 3).

The second approach employs analytic expressions (Eqs. 1–9 in Methods) that couple equations from atmospheric fluid dynamics to equations from wind farm fluid dynamics. The equations from atmospheric fluid dynamics concern steady-state, horizontal, large-scale flows under neutral conditions above an infinite homogeneous surface [42–44]. They specifically describe turbulent Ekman layers and provide an approximate expression to relate the large-scale flow (geostrophic flow and Ekman layer) with the small-scale flow (surface layer, where turbines are located). The equations from wind farm fluid dynamics concern instead steady-state, horizontal flows under neutral conditions within and over an infinite wind farm [11,45]. In this case, their derivation neglects any effect of the Coriolis force and focuses on smaller spatial scales. This analysis provides an equivalent surface roughness for the effect of a large wind farm on the overlying atmospheric boundary

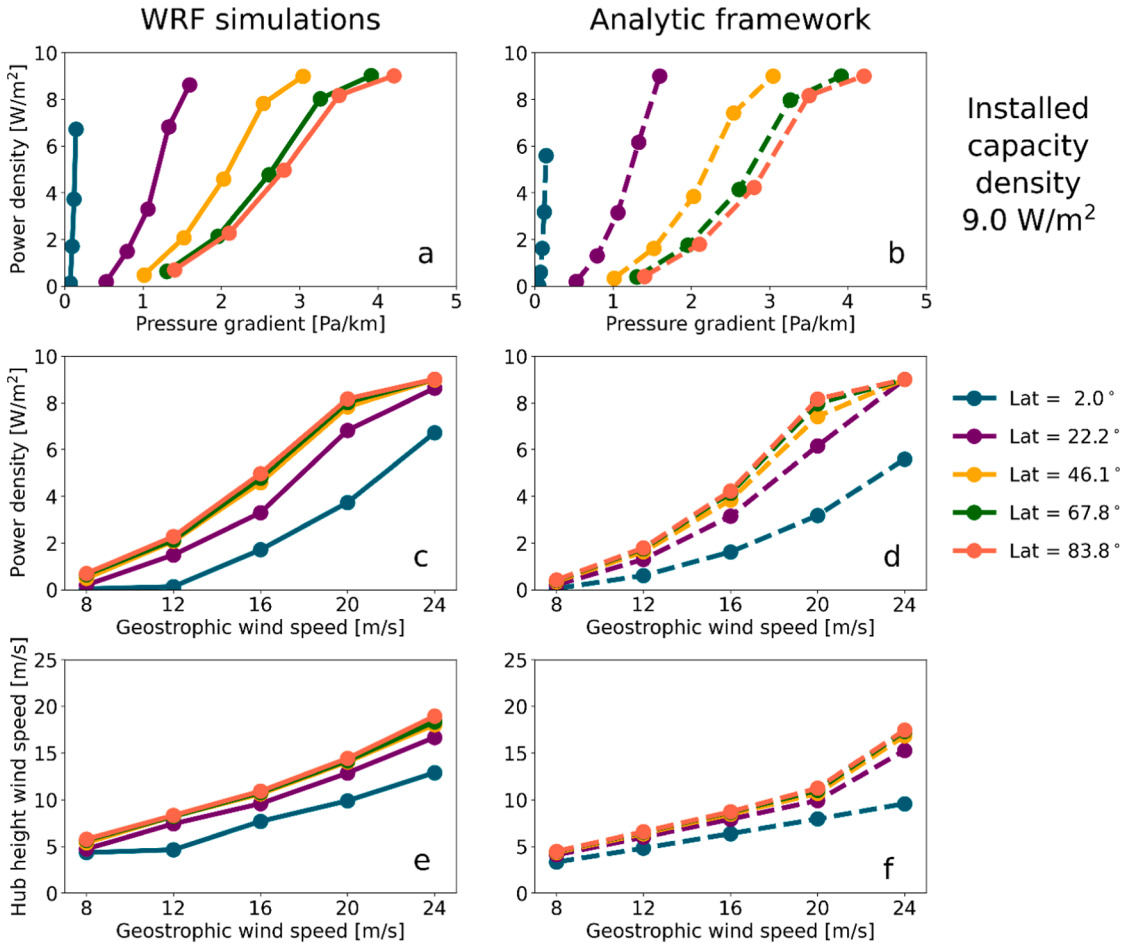

Fig. 2. Power density and hub height wind speed for a large wind farm with an installed capacity density of 9 W/m^2 as a function of the Coriolis parameter, f, (latitude-dependent) and pressure gradient or geostrophic wind. Left panels (a, c, e) show results from the atmospheric simulations conducted with the Weather Research and Forecasting (WRF) simulation tool, whereas right panels (b, d, f) show results from the analytic expressions. Panels a and b show power density values as a function of pressure gradient, panels c and d show the power density values as a function of geostrophic wind speed, and panels e and f show hub height wind speed as a function of geostrophic wind speed. The results are provided for the set of Coriolis parameters 0.05, 0.55, 1.05, 1.35, and 1.45 · 10^{-4} rad/s^{-1}, which corresponds to the set of latitudes 2.0, 22.2, 46.1, 67.8, and 83.8° N. The hypothetical wind farm considered has an installed capacity density of 9 W/m^2. The analytic treatment uses standard literature values for coefficients and includes no tunable parameters.

layer. Here, we combine the equations from these two separate fields, and develop a closed-form system that relates the power density generated by an infinite wind farm to the geostrophic flow characterized by the pressure gradient and a Coriolis parameter (Eqs. 1–9 in Methods). The same set of these two parameters and the same wind farm used in the numerical analysis are employed in this analytic framework to have a comparable investigation of the wind farm performance.

3. Methods

3.1. Atmospheric simulations

The idealized simulations are conducted with the Weather Research and Forecasting (WRF) simulation tool [38], version 4.2.1 [46,47]. We use the native parametrization for the wind turbines, which represents them as sinks of momentum (the turbine drag proportional to the thrust coefficient data) and sources of turbulence kinetic energy (the fraction of kinetic energy not transferred into electricity) [39,40,41]. We use the default value for the correction factor (=0.25) to the turbulent kinetic energy produced by the turbines. The WRF model domain has a horizontal size of 50 × 50 km^2 with a uniform grid resolution of 1 km. The vertical dimension is 10 km with a variable, stretching resolution, finer at the bottom (23 levels in the first 1 km) and coarser at the top (37 levels in the remaining 9 km). Here, we consider a wind farm with a set of Vestas V164-9.0 MW (see Supplementary Note 1), one of the largest wind turbines currently available, with a hub height of 130 m, arranged on a uniform grid with spacing of 1000 m. We populate this uniform grid to obtain and study two different installed capacity densities: 9 W/m^2, where all the grid cells contain a turbine resulting in an aligned layout with a turbine density of 1 km^{-2}, and 4.5 W/m^2, where the grid cells are populated alternatively resulting in a staggered layout with a turbine density of 0.5 km^{-2}. We parametrize this wind farm on the 8 layers intersecting the rotor area in a doubly periodic domain that we use to emulate an infinite wind farm. On this domain, we specify a set of vertically uniform geostrophic wind values and constant Coriolis parameters (f-plane approximation). The set of Coriolis parameters is 0.05, 0.55, 1.05, 1.35, and 1.45 · 10^{-4} rad/s^{-1}, which corresponds to the set of latitudes 2.0, 22.2, 46.1, 67.8, and 83.8° N. These settings in the boundary conditions implicitly assume a driving constant pressure-gradient field for each of the considered combinations (see Eq. (1)). The bottom boundary is defined as a sea surface with a roughness length of 10^{-4} m. We use a dry atmosphere with no surface heat, no radiation, and no moisture fluxes. The planetary boundary layer physics is parameterized using the Mellor–Yamada–Nakanishi–Niino (MYNN) Level-2.5 model [48,49]. Each simulation is run with a time step of 10 s and for a total of 7 days in order to reach stationary conditions. Resulting variables are then averaged horizontally and over the last 12 h. The power produced by each turbine is calculated with the power curve provided by the manufacturer (see Supplementary Fig. 1) according to the wind speed at the turbine-containing levels where the turbine is located.

3.2. Analytic framework

The analytic framework includes equations from the atmospheric fluid dynamics and wind farm fluid dynamics. The equations from atmospheric fluid dynamics concern steady-state, horizontal, large-scale flows under neutral conditions above an infinite homogeneous surface with roughness z_0 [42–44]. First, we recall the governing equations of the geostrophic flow, i.e., the momentum equations [35]:

$$-fV_g = -\frac{1}{\rho}\frac{\partial p}{\partial x}, fU_g = -\frac{1}{\rho}\frac{\partial p}{\partial y}, \tag{1}$$

where U_g and V_g are the geostrophic wind components (G is the modulus), p the pressure, ρ the density, and f the Coriolis parameter. The Coriolis parameter is given by $2\Omega\sin\varphi$, where Ω is the rotation rate of the Earth ($7.2921 \cdot 10^{-5}$ rad/s), and φ the latitude. In the Ekman layer, mechanical turbulence becomes important, and the resulting momentum equations then become [36]:

$$-fv = -\frac{1}{\rho}\frac{\partial p}{\partial x} - \frac{\partial(\overline{u'w'})}{\partial z}, fu = -\frac{1}{\rho}\frac{\partial p}{\partial y} - \frac{\partial(\overline{v'w'})}{\partial z} \tag{2}$$

where u and v are the mean wind components, and $\overline{u'w'}$ and $\overline{v'w'}$ are the turbulent fluxes (also called Reynolds stresses). Substituting the pressure-gradient terms of Eq. (2) with the Coriolis force terms from Eq. (1), the equations of motion can be written as [36]:

$$f(v - V_g) = \frac{\partial(\overline{u'w'})}{\partial z}, f(u - U_g) = -\frac{\partial(\overline{v'w'})}{\partial z}. \tag{3}$$

From these governing equations, Blackadar and Tennekes [42] derived, for the case of large Rossby numbers, $Ro = G/(fz_0)$, two kinds of self-similar solutions, one valid only in the Ekman layer well outside the surface layer and another valid inside the surface layer [44]. By matching those solutions in a region of overlap, they derived the following expressions:

$$\frac{U_g}{u_*} = \frac{1}{\kappa}\ln\left(\frac{u_*}{fz_0}\right) - 4, \frac{V_g}{u_*} = -12, \tag{4}$$

$$\frac{G}{u_*} = \sqrt{\left(\frac{U_g}{u_*}\right)^2 + \left(\frac{V_g}{u_*}\right)^2} = \sqrt{\left(\frac{1}{\kappa}\ln\left(\frac{u_*}{fz_0}\right) - 4\right)^2 + 12^2}, \tag{5}$$

where u_* is the surface friction velocity and κ the Von Kármán constant (≈ 0.4). The resistant constants (4 and 12) on the right-hand side of Eq. (4) are derived in Refs. [42,44]. These equations relate the large-scale flow (geostrophic flow and Ekman layer) to the small-scale flow (surface layer, where turbines are located).

The equations from wind farm fluid dynamics concern instead steady-state, horizontal flows under neutral conditions within and over an infinite wind farm [11,45]. In this case, the derivation neglects any effect of the Coriolis force and focuses on smaller spatial scales. This analysis provides an equivalent surface roughness, $z_{0,wf}$, for the effect of a large wind farm on the overlying atmospheric boundary layer [11]:

$$z_{0,wf} = z_H\left(1 + \frac{D}{2z_H}\right)^{\nu_w^*/1+\nu_w^*} \exp\left\{-\left\{\frac{c_{ft}}{2\kappa^2} + \left\{\ln\left[\frac{z_H}{z_0}\left(1 - \frac{D}{2z_H}\right)^{\nu_w^*/1+\nu_w^*}\right]\right\}^{-2}\right\}^{-0.5}\right\}, \tag{6}$$

where D and z_H are the turbine diameter and hub height, respectively, z_0 the actual surface roughness of the underlying terrain, and

$$\nu_w^* = \frac{\sqrt{0.5c_{ft}}U_H D}{\kappa u_{*,wf} z_H}, \tag{7}$$

$$c_{ft} = \frac{\pi C_T}{4 s_x s_y}, \tag{8}$$

where U_H is the hub-height wind speed, $u_{*,wf}$ the equivalent surface

friction velocity generated by the wind farm, C_T is the thrust coefficient provided by the manufacturer (see Supplementary Fig. 1), and s_x and s_y are the horizontal nondimensional spacings. For the case of aligned layout and installed capacity density of 9 W/m^2, $s_x = s_y = 1000/D = 6.1$, whereas for the case of staggered layout and installed capacity density of 4.5 W/m^2, $s_x = s_y = \sqrt{2}\cdot 1000/D = 8.6$.

The hub-height wind speed is calculated according to [11]:

$$U_H = \frac{u_{*,wf}}{\kappa}\ln\left[\frac{z_H}{z_{0,wf}}\left(1+\frac{D}{2z_H}\right)^{\nu_w^*/1+\nu_w^*}\right] \quad (9)$$

Here, we combine Eq. (5) with Eqs. 6–9 to provide a closed-form system that relates the influence of geostrophic wind and Coriolis parameter (latitude-dependent) with the wind farm power density. z_0 and u_* in Eq. (5) are replaced with $z_{0,wf}$ and $u_{*,wf}$ to account for the effect of the wind farm on the Ekman layer. The system represented by Eqs. 5–9, with unknowns $u_{*,wf}$, $z_{0,wf}$, ν_w^*, c_{ft} and U_H, can be solved iteratively and provides a value for U_H, with which we calculate the power produced according to the power curve given by the manufacturer (see Supplementary Fig. 1).

4. Results

Figs. 2 and 3 show the power density and hub height wind speed values resulting from the WRF simulations and the analytic expressions for a set of pressure gradients and Coriolis parameters. Because pressure gradients and Coriolis parameters define geostrophic winds, these results can also be plotted in terms of the geostrophic winds. The numerical model and analytic expressions provide results with a high level of agreement, demonstrating that the mechanisms at play in the analytic solution largely govern the behavior of the fluid dynamical model (see Supplementary Note 5 for further comparison). Both the numerical fluid dynamical and the analytic expressions clearly show, in panels a, b, c and d of Figs. 2 and 3, the effect of the pressure gradient and the Coriolis parameter on wind farm power density. In addition to well capturing the energetics, the analytic framework also provides consistent predictions of hub height wind speed and its dependence on geostrophic wind and Coriolis parameter, as plotted in panels e and f of Figs. 2 and 3.

Pressure gradients have a substantial direct effect on power density: higher pressure gradients promote higher energy availability and, consequently, higher power density. The power densities for mid and high latitudes (46.1, 67.8, and 83.8° N) reach their maximum value of 4.5 and 9 W/m^2 for combinations of pressure gradient and Coriolis forces yielding a geostrophic wind of 20 and 24 m/s, respectively, which means that the turbines are operating at their maximum power of 9 MW, given that the turbine densities are 0.5 and 1 km^{-2}. For higher geostrophic winds, the power density evidently remains constant at that maximum value, up to the geostrophic wind for which the hub height wind speed reaches the wind turbine cut-off wind speed. In the wind farm with lower installed capacity density, for the same geostrophic wind, more power is extracted per turbine but less power per unit land. In fact, as the installed capacity density decreases, turbines are sparser and less affected by wakes of upstream turbines resulting in higher energy extraction, however over a larger area. The 4.5 and 9 W/m^2 maximum values of power density would be reached at lower latitudes with lower pressure gradients, because the pressure gradient forces are opposed by Coriolis forces to a lesser degree. At a constant pressure gradient, potential power density decreases with increasing latitude. Because the rate of change in the Coriolis parameter with latitude is proportional to the cosine of latitude, the potential power density varies sensitively with latitude at low latitudes, and less sensitively at high latitudes.

Note that the analytic expressions are derived under the assumptions of large Rossby number and geostrophic flow conditions; these

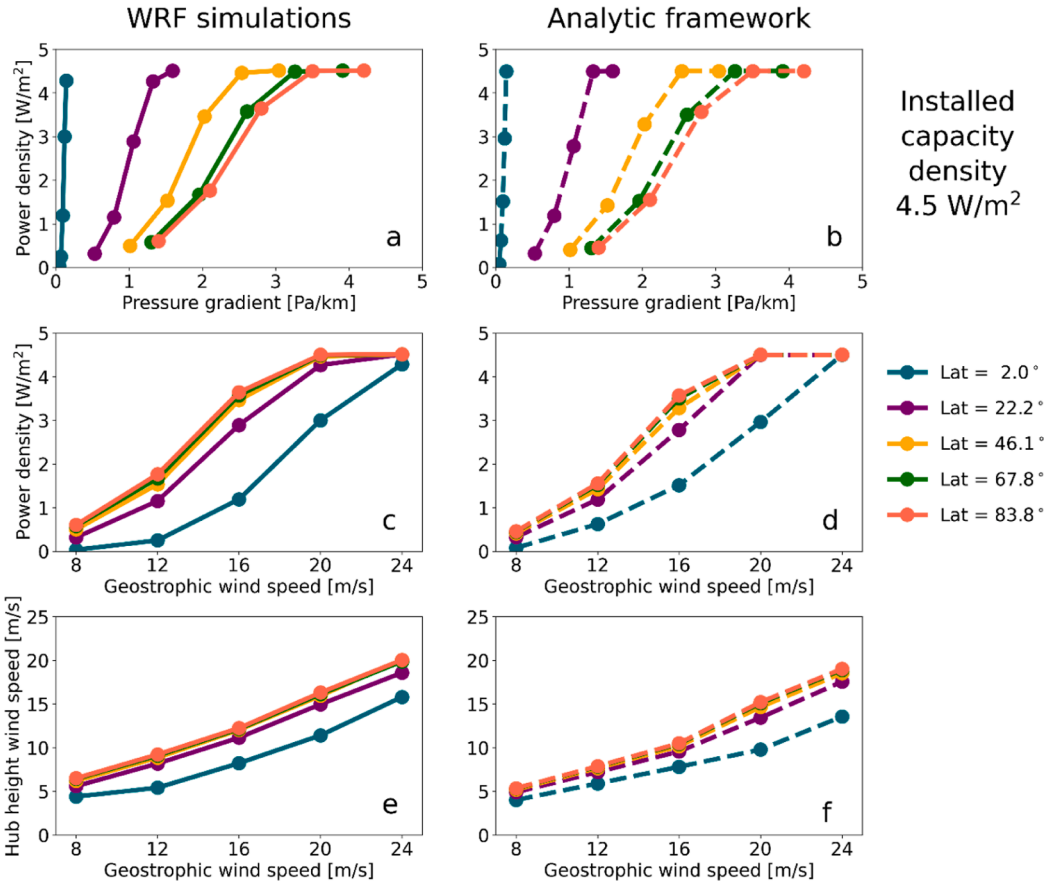

Fig. 3. Power density and hub height wind speed for a large wind farm with an installed capacity density of 4.5 W/m^2 as a function of the Coriolis parameter, f, (latitude-dependent) and pressure gradient or geostrophic wind. Left panels (a, c, e) show results from the atmospheric simulations conducted with the Weather Research and Forecasting (WRF) simulation tool, whereas right panels (b, d, f) show results from the analytic expressions. Panels a and b show power density values as a function of pressure gradient, panels c and d show the power density values as a function of geostrophic wind speed, and panels e and f show hub height wind speed as a function of geostrophic wind speed. The results are provided for the set of Coriolis parameters 0.05, 0.55, 1.05, 1.35, and 1.45 · 10^{-4} rad/s^{-1}, which corresponds to the set of latitudes 2.0, 22.2, 46.1, 67.8, and 83.8° N. The hypothetical wind farm considered has an installed capacity density of 4.5 W/m^2. The analytic treatment uses standard literature values for coefficients and includes no tunable parameters.

assumptions break down for the low Coriolis parameter values present near the equator and for low values of geostrophic wind (see Methods in Sec. 3). This may explain the discrepancies between the analytic and numerical results that we observe for a latitude of 2° N and, to a smaller degree, for geostrophic wind speeds of 8 and 12 m/s. On the other hand, the numerical simulations rely on the solution of the full continuity, momentum and energy equations and do not need assumption such as large Rossby number or geostrophic flow conditions. Their predictions are therefore expected to hold valid also for near-equatorial regions and low values of geostrophic wind.

5. Geographic distribution of potential power density

We now aim to estimate the potential power density of a representative large wind farm (for this case, with an installed capacity density of 9 W/m^2 and the same characteristics used in the numeric and analytic frameworks) that would be generated on a given location on the Earth's surface. That is, with the analytic framework previously illustrated, we aim to estimate the geographic distribution of potential power density over the Earth and compare it with available previous estimates. To conduct this analysis, we use the spatial distribution of the Coriolis parameter and geostrophic wind. The Coriolis parameter is straightforward to calculate given the latitude, whereas reanalysis data are used to calculate geographic distribution of the geostrophic wind speed. Here, we use the ERA5 reanalysis data [50], and we obtained the hourly averaged wind speed during 2019 at 2 km altitude above ground level. This altitude can be considered representative of mean geostrophic flow conditions, given that the height of the planetary boundary layers ranges between 100 and 2000 m [51,52]. We then average the power density obtained with the hourly averaged wind speed to calculate the annual potential power density (see also Supplementary Note 4). Two surface roughness values, 10^{-1} and 10^{-4} m, are selected for land and sea, respectively, for the estimation of the worldwide potential power density. However, the equivalent surface roughness, $z_{0,wf}$, used in our analytic expressions is only slightly sensitive to the actual surface roughness and mainly affected by turbine dimensions and operating conditions. In fact, the turbines represent the dominant surface roughness elements. Further, our study aims to identify primary underlying mechanisms, and is not intended to serve as a detailed resource estimation. For example, we used reanalysis data for a single year (2019), which could reasonably be expected to vary by ± 6% of the long-term multi-year average [53]. Moreover, greater time resolutions (e.g., 10-minute average) would provide a more accurate estimate of the average power density because power scales with wind speed cubed.

Fig. 4 illustrates the geographic distribution of the Coriolis parameter, the mean geostrophic wind speed, and the resulting power density of a large wind farm estimated with the analytic framework. We observe that for vast areas of the Earth's surface the potential power density is below 1 W/m^2, whereas only a few regions (e.g., North Atlantic Ocean, North Pacific Ocean, and southern mid latitudes over the Indian and Pacific Oceans) have favorable geostrophic flow conditions that can sustain, on average, a much higher kinetic energy replenishment rate and power density. We observe also that regions with similar geostrophic wind speeds (e.g., Pacific Ocean near the equator and at mid latitudes, or North Atlantic Ocean and Caribbean Sea) do not necessarily have similar power densities if one of the regions is at lower latitudes.

Given the potential power density estimates for our representative large wind farm, we compare them with the estimates of previous studies, both at the regional and global scale. At the global scale, our estimations give a mean power density of 1.28 W/m^2, consistent with studies that looked at the global mean of power density and its limits [13,54–56], estimating it to be about 1 W/m^2. Even though our numerical value for the global mean is consistent and could be valid as a first-order estimate, we underline the fact that our problem formulation

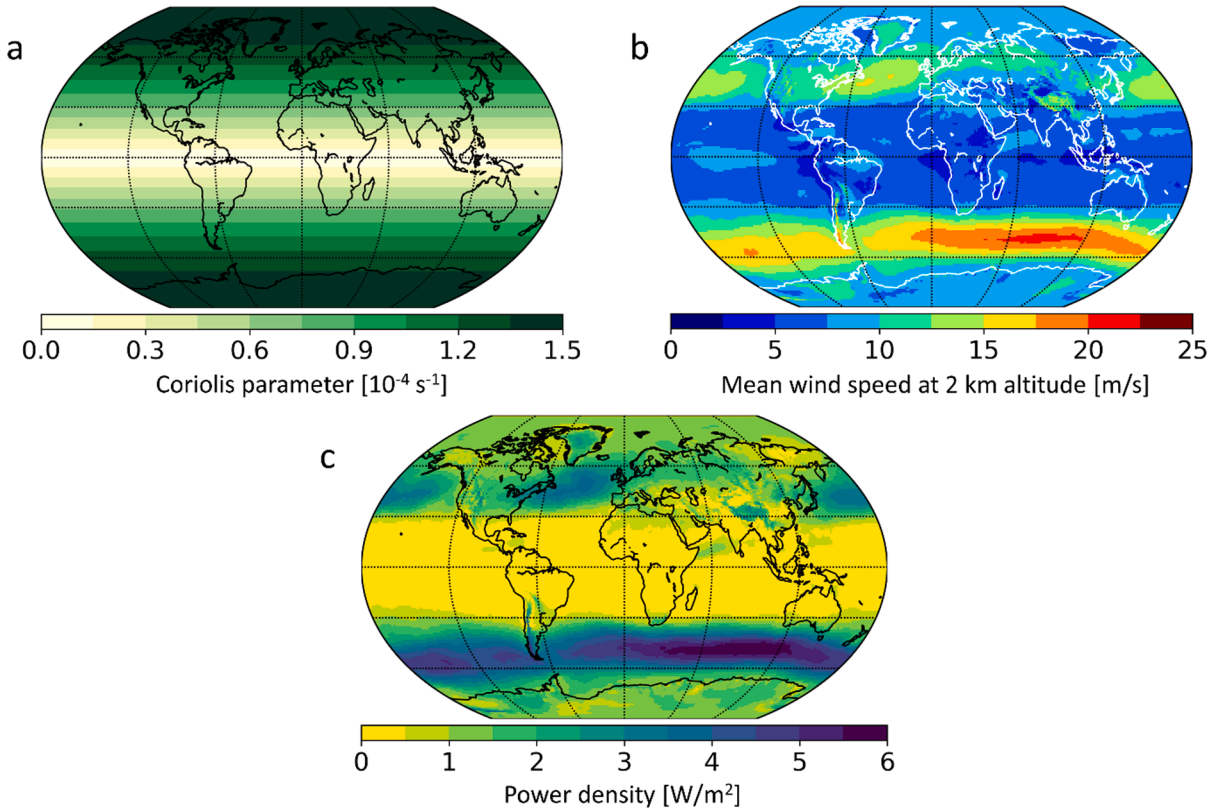

Fig. 4. Geographic distribution of the Coriolis parameter (a), geostrophic wind speed (b), and resulting power density for a large wind farm (c). The Coriolis parameter depends on the latitude and is straightforward to calculate. The geostrophic wind is estimated for 2019 from ERA5 reanalysis data at 2 km altitude above ground level. Given the spatial distribution of Coriolis parameter and geostrophic wind speed, the power density can be estimated with the analytic expressions.

does not consider a global energy balance and such scalability may be improper. We find, however, consistent regional estimates for which our framework is more applicable. For example, Miller *et al.* [16] conducted an extensive analysis of the power density for all the operational wind power plants in the United States. They found a mean power density of 0.9 W/m^2, whereas a value of 0.5 W/m^2 for the largest wind farms. Considering that most of wind power plants analyzed are located in the central and midwestern United States, our estimates give a range of 1 to 1.5 W/m^2 for the same regions. Possner *et al.* [18] studied with a global climate model how much power a large wind farm would generate over the North Atlantic Ocean. They found mean power density values of 6 W/m^2, and they argue that the surface heat flux played a crucial role in sustaining high rates of downward kinetic energy transport. Here, we find, over the same region, a power density in the range from 2 to 4 W/m^2, which is lower than their estimate but overall consistent given the higher geostrophic winds and that our formulation does not account for surface heat fluxes.

6. Discussion and conclusions

In this study, we have characterized the effect of pressure-gradient and Coriolis forces on the performance of large-scale wind farms by means of both atmospheric simulations and analytic expressions. We have shown that higher pressure gradients promote higher power density and that, for the same pressure gradient, maximum power density at lower latitudes is higher than at higher latitudes. Previous studies that aimed to characterize power density in large wind farms did not consider pressure gradient or Coriolis forces [34], or used pre-turbine climatology to estimate power generation without accounting for the feedback effect of the wind farm on the atmosphere dynamics [14]. In contrast, our analytic framework captures the full wind farm-atmosphere interaction and provides a mechanistic understanding of the energy extraction of large wind farms confirmed by the results of our framework comparable with the atmospheric simulations.

Our problem formulation has been defined for an idealized scenario with an infinite wind farm over a flat terrain assuming neutral atmospheric conditions and dry air. We emphasize that other phenomena, such as evaporation, precipitation, heat fluxes, stratification, or inversion layers, play a crucial role in the momentum and energy transport within and above the planetary boundary layer [23,24,57,58]. For example, cumulus-driven vertical advection of horizontal momentum is particularly important in the tropics [59,60]. Terrain topography is also known to alter the wind flow characteristics at the local scale [25,27]. When horizontal temperature gradients are present, baroclinicity is expected to change geostrophic winds with height [61]. Nonetheless, we deem our assumptions justified for a first-order characterization of the energy exchange mechanisms in large wind power plants.

Further, the energy extraction rate and its transport mechanisms predicted in our analysis are not expected to be affected by the type of wind turbines. A recent body of research has investigated whether vertical axis wind turbines have any advantage over horizontal axis ones. Whereas it is well established that stand-alone vertical axis wind turbines have lower efficiencies [62], small clusters of these same turbines have been shown to have higher power densities than large wind power plants of horizontal axis wind turbines [63]. We attribute these last findings to the different scales used for comparing the two technologies (wind farm of tens of meters as opposed to kilometers), and the fact that small scale facilities do not reach fully-developed regime as did the ones investigated in the present study. Nevertheless, in our formulation there is no assumption regarding the geometry of the wind turbines. In fact, the parametrization of wind turbines occurs through momentum sinks in the atmospheric simulations and equivalent surface roughness in the analytic framework, which would apply equally to both technologies.

Our findings show that there is not a universal limit to power density for large wind farms, as suggested in previous studies [14,64]. In fact, we find that the power density is strongly dependent, to a first-order approximation, on the local pressure gradient and Coriolis parameter. We have shown, in both numerical and analytic frameworks, that a representative large wind farm can have a power density much higher than 1 W/m^2 if local atmospheric conditions provide a larger pressure-gradient force available to accelerate air in the boundary layer. The representative wind farm that we have considered has an installed capacity density of 9 W/m^2 (relatively high for modern, large installations), and we have shown that in some locations (e.g., southern mid latitudes over the Indian and Pacific Oceans) the power density could reach values of about 6 W/m^2 (an outcome that is excluded according to previous studies [14,16,64]). We stress again the fact that our problem formulation is thought out for regional scales and does not account for a global energy balance. Estimations of power densities at a global scale may therefore incur wind power saturation and global geophysical limits [13,56].

The need of a deeper understanding and theoretical formulations has been emphasized as one of the challenges of wind energy science for large wind power plants [9,10]. Our analytic framework, represented by Eqs. 1–9, relates power density of large wind farms to local pressure gradient forces and Coriolis parameters, providing a better understanding of how these systems function and how much energy they can generate on average. These equations describe the interactions that occur through the Ekman layer between the small-scale surface layer, where the wind turbines operate, and the large-scale pressure fields. They show that the energy and momentum removed from the boundary layer by wind turbines is replenished from energy and momentum derived primarily from pressure-gradient forces within the Ekman layer, and not from the overlying free troposphere (see Supplementary Notes 2 and 3). Our analysis and findings can be used by wind farm developers to help understand the basic principles underlying the assessment of economic feasibility of large wind farms. Also, our results will help inform policy makers and energy system planners who seek to understand the potential contributions of wind power to future energy systems.

7. Data availability

Research data required to reproduce the work reported in the manuscript is available in the GitHub repository at https://github.com/eantonini/Power_density_of_large_wind_farms.

CRediT authorship contribution statement

Enrico G.A. Antonini: Conceptualization, Methodology, Software, Validation, Formal analysis, Investigation, Data curation, Writing - original draft, Writing - review & editing, Visualization, Project administration. **Ken Caldeira:** Conceptualization, Validation, Formal analysis, Resources, Writing - review & editing, Supervision, Project administration, Funding acquisition.

Declaration of Competing Interest

The authors declare that they have no known competing financial interests or personal relationships that could have appeared to influence the work reported in this paper.

Acknowledgements

This work was supported by a gift from Gates Ventures LLC to the Carnegie Institution for Science.

Appendix A. Supplementary data

Supplementary data to this article can be found online at https://doi.org/10.1016/j.apenergy.2020.116048.

References

[1] International Energy Agency (IEA), Global Energy & CO2 Status Report 2018, 2019.
[2] Davis SJ, et al. Net-zero emissions energy systems. Science Jun. 2018;360(6396).
[3] Jacobson MZ. Review of solutions to global warming, air pollution, and energy security. Energy Environ. Sci. 2009;2:148–73.
[4] Lewis JI, Wiser RH. Fostering a renewable energy technology industry: An international comparison of wind industry policy support mechanisms. Energy Policy 2007;35(3):1844–57.
[5] Stokes LC, Warshaw C. Renewable energy policy design and framing influence public support in the United States. Nat. Energy 2017;2(8):1–6.
[6] Krohn S, Damborg S. On public attitudes towards wind power. Renew. Energy Jan. 1999;16(1–4):954–60.
[7] Rand J, Hoen B. Thirty years of North American wind energy acceptance research: What have we learned? Energy Res. Soc. Sci. 2017;29:135–48.
[8] International Energy Agency (IEA), World Energy Outlook 2018, 2018.
[9] Veers P, et al. Grand challenges in the science of wind energy. Science 2019;443 (6464).
[10] Meneveau C. Big wind power: seven questions for turbulence research. J. Turbul. 2019;20(1):2–20.
[11] Calaf M, Meneveau C, Meyers J. Large eddy simulation study of fully developed wind-turbine array boundary layers. Phys. Fluids 2010;22(1):1–16.
[12] Hamilton N, Kang HS, Meneveau C, Cal RB. Statistical analysis of kinetic energy entrainment in a model wind turbine array boundary layer. J. Renew. Sustain. Energy 2012;4(6).
[13] Marvel K, Kravitz B, Caldeira K. Geophysical limits to global wind power. Nat. Clim. Chang. 2013;3(2):118–21.
[14] Miller LM, et al. Two methods for estimating limits to large-scale wind power generation. Proc. Natl. Acad. Sci. U. S. A. 2015;112(36):11169–74.
[15] Miller LM, Kleidon A. Wind speed reductions by large-scale wind turbine deployments lower turbine efficiencies and set low generation limits. Proc. Natl. Acad. Sci. U. S. A. 2016;113(48):13570–5.
[16] Miller LM, Keith DW. Observation-based solar and wind power capacity factors and power densities. Environ. Res. Lett. 2018;13(10).
[17] Volker PJH, Hahmann AN, Badger J, Jørgensen HE. Prospects for generating electricity by large onshore and offshore wind farms. Environ. Res. Lett. 2017;12 (3).
[18] Possner A, Caldeira K. Geophysical potential for wind energy over the open oceans. Proc. Natl. Acad. Sci. U. S. A. 2017;114(43):11338–43.
[19] Wu Y-T, Porté-Agel F. Atmospheric turbulence effects on wind-turbine wakes: An LES study. Energies 2012;5(12):5340–62.
[20] Stevens RJAM, Meneveau C. Flow Structure and Turbulence in Wind Farms. Annu. Rev. Fluid Mech. 2017;49(1):311–39.
[21] Antonini EGA, Romero DA, Amon CH. Analysis and Modifications of Turbulence Models for Wind Turbine Wake Simulations in Atmospheric Boundary Layers. J. Sol. Energy Eng. 2018;140(3):031007.
[22] Antonini EGA, Romero DA, Amon CH. Improving CFD Wind Farm Simulations incorporating Wind Direction Uncertainty. Renew. Energy 2019;133:1011–23.
[23] Hansen KS, Barthelmie RJ, Jensen LE, Sommer A. The impact of turbulence intensity and atmospheric stability on power deficits due to wind turbine wakes at Horns Rev wind farm. Wind Energy 2012;15(1):183–96.
[24] Abkar M, Porté-Agel F. Influence of atmospheric stability on wind-turbine wakes: A large-eddy simulation study. Phys. Fluids 2015;27(3).
[25] Han X, Liu D, Xu C, Shen WZ. Atmospheric stability and topography effects on wind turbine performance and wake properties in complex terrain. Renew. Energy 2018;126:640–51.
[26] Fitch AC, Lundquist JK, Olson JB. Mesoscale influences of wind farms throughout a diurnal cycle. Mon. Weather Rev. 2013;141(7):2173–98.
[27] Mann J, et al. Complex terrain experiments in the New EuropeanWind Atlas. Philos. Trans. R. Soc. A Math. Phys. Eng. Sci. 2017;375(2091).
[28] Røkenes K, Krogstad PÅ. Wind tunnel simulation of terrain effects on wind farm siting. Wind Energy 2009;12(4):391–410.
[29] Churchfield MJ, Lee S, Michalakes J, Moriarty PJ. A numerical study of the effects of atmospheric and wake turbulence on wind turbine dynamics. J. Turbul. 2012;13 (May):N14.
[30] Wu Y-T, Porté-Agel F. Simulation of Turbulent Flow Inside and Above Wind Farms: Model Validation and Layout Effects. Boundary-Layer Meteorol. 2012;146(2): 181–205.
[31] Stevens RJAM. Dependence of optimal wind turbine spacing on wind farm length. Wind Energy Apr. 2016;19(4):651–63.
[32] Antonini EGA, Romero DA, Amon CH. Continuous adjoint formulation for wind farm layout optimization: A 2D implementation. Appl. Energy 2018;228:2333–45.
[33] Antonini EGA, Romero DA, Amon CH. Optimal design of wind farms in complex terrains using computational fluid dynamics and adjoint methods. Appl. Energy 2020;261:114426.
[34] Luzzatto-Fegiz P, Caulfield CCP. Entrainment model for fully-developed wind farms: Effects of atmospheric stability and an ideal limit for wind farm performance. Phys. Rev. Fluids 2018;3(9).
[35] Mak M. Atmospheric Dynamics. Cambridge University Press; 2011.
[36] Jacobson MZ. Fundamentals of Atmospheric Modeling. Cambridge University Press; 2005.
[37] Cal RB, Lebrón J, Castillo L, Kang HS, Meneveau C. Experimental study of the horizontally averaged flow structure in a model wind-turbine array boundary layer. J. Renew. Sustain. Energy 2010;2(1).
[38] Powers JG, et al. The weather research and forecasting model: Overview, system efforts, and future directions. Bull. Am. Meteorol. Soc. 2017;98(8):1717–37.
[39] Fitch AC, et al. Local and mesoscale impacts of wind farms as parameterized in a mesoscale NWP model. Mon. Weather Rev. 2012;140(9):3017–38.
[40] Fitch AC. Notes on using the mesoscale wind farm parameterization of Fitch et al. (2012) in WRF. Wind Energy 2016;19(9):1757–8.
[41] Lee JCY, Lundquist JK. Evaluation of the wind farm parameterization in the Weather Research and Forecasting model (version 3.8.1) with meteorological and turbine power data. Geosci. Model Dev. 2017;10(11):4229–44.
[42] Blackadar AK, Tennekes H. Asymptotic Similarity in Neutral Barotropic Planetary Boundary Layers. J. Atmos. Sci. 1968;25(6):1015–20.
[43] Tennekes H, Lumley JL. A first course in turbulence. MIT press 1972.
[44] Tennekes H. The Logarithmic Wind Profile. J. Atmos. Sci. 1973;30(2):234–8.
[45] Meneveau C. The top-down model of wind farm boundary layers and its applications. J. Turbul. 2012;13:1–12.
[46] W. C. Skamarock et al., A Description of the Advanced Research WRF Version 4, 2019.
[47] "WRF Version 4.2.1," 2020. [Online]. Available: https://github.com/wrf-model/WRF/releases/tag/v4.2.1.
[48] Nakanishi M, Niino H. An improved Mellor-Yamada Level-3 model with condensation physics: Its design and verification. Boundary-Layer Meteorol. 2004; 112(1):1–31.
[49] Nakanishi M, Niino H. Development of an improved turbulence closure model for the atmospheric boundary layer. J. Meteorol. Soc. Japan 2009;87(5):895–912.
[50] Copernicus Climate Change Service (C3S), "ERA5: Fifth generation of ECMWF atmospheric reanalyses of the global climate," Copernicus Climate Change Service Climate Data Store (CDS), 2017. [Online]. Available: https://cds.climate.copernicus.eu/cdsapp#!/home.
[51] Panofsky HA, Dutton JA. Atmospheric Turbulence: Models and Methods for Engineering Applications. New York, New York, USA: John Wiley & Sons; 1984.
[52] Hennemuth B, Lammert A. Determination of the atmospheric boundary layer height from radiosonde and lidar backscatter. Boundary-Layer Meteorol. 2006;120 (1):181–200.
[53] Pryor SC, Shepherd TJ, Barthelmie RJ. Interannual variability of wind climates and wind turbine annual energy production. Wind Energy Sci. 2018;3(2):651–65.
[54] Gustavson MR. Limits to wind power utilization. Science 1979;204(4388):13–7.
[55] Peixoto JP, Oort AH. Physics of climate. American Institute of Physics; 1992.
[56] Jacobson MZ, Archer CL. Saturation wind power potential and its implications for wind energy. Proc. Natl. Acad. Sci. U. S. A. 2012;109(39):15679–84.
[57] Allaerts D, Meyers J. Large eddy simulation of a large wind-turbine array in a conventionally neutral atmospheric boundary layer. Phys. Fluids 2015;27(6).
[58] Rajewski DA, et al. Crop wind energy experiment (CWEX): Observations of surface-layer, boundary layer, and mesoscale interactions with a wind farm. Bull. Am. Meteorol. Soc. 2013;94(5):655–72.
[59] Houze RA. A Climatological Study of Vertical Transports by Cumulus-Scale Convection. J. Atmos. Sci. Sep. 1973;30(6):1112–23.
[60] Carr MT, Bretherton CS. Convective momentum transport over the tropical pacific: Budget estimates. J. Atmos. Sci. 2001;58(13):1673–93.
[61] Floors R, Peña A, Gryning S-E. The effect of baroclinicity on the wind in the planetary boundary layer. Q. J. R. Meteorol. Soc. 2015;141(687):619–30.
[62] Pope K, Dincer I, Naterer GF. Energy and exergy efficiency comparison of horizontal and vertical axis wind turbines. Renew. Energy 2010;35(9):2102–13.
[63] Dabiri JO. Potential order-of-magnitude enhancement of wind farm power density via counter-rotating vertical-axis wind turbine arrays. J. Renew. Sustain. Energy 2011;3(4).
[64] Adams AS, Keith DW. Are global wind power resource estimates overstated? Environ. Res. Lett. 2013;8(1).